Electron Emission from Solids Irradiated with Swift Ion Beams

Hermann Rothard* and Benoit Gervais

Centre Interdisciplinaire de Recherche Ions Lasers
UMR 6637 (CEA/CNRS/ENSICAEN/Université de Caen)
CIRIL-Ganil, Boulevard Henri Becquerel
BP 5133, F-14070 Caen Cedex 05, France

Abstract

We present basic features, important results obtained so far, and open questions on electron ejection from solids induced by swift ion beams in the "electronic stopping" regime, where the transfer of kinetic energy to target electrons dominates over effects related to potential energy or elastic stopping. Topics include primary ionization in binary collisions, transport of fast and slow electrons, multiple collision sequences (Fermi shuttle), collective excitations (wake, plasmons), effects related to strong perturbation (high charge effects on primary ionization and electron transport, multiple ionization), Auger electron spectroscopy (track potential, electronic temperatures), statistics and correlated emission of electrons, electron ejection in channeling, and charging effects in insulating targets.

Contents

1 Introduction: Present Knowledge **498**

2 Experimental Techniques: New Developments **500**

3 Overview: Basic Mechanisms **501**

4 Primary Ionization, Fast Electron Transport and Collision Sequences **505**

* E-mail: rothard@ganil.fr

5 Low Energy Electrons: Collective Excitations **507**

6 Electron Yields: Scaling Laws **508**

7 Strong Perturbation: High Charge Effects **511**

8 Auger Electrons: Electronic Temperatures **514**

9 Insulators: Charging Effects **516**

10 Channeling and Emission Statistics **517**

11 Other Intriguing Topics: An Open End **518**

Acknowledgements **519**

References **520**

1. Introduction: Present Knowledge

The major part of the energy deposited in matter by swift ions in the "electronic stopping" regime leads to ionization of the target atoms. In condensed matter, ejected electrons may then suffer elastic scattering or inelastic scattering by target atoms during their transport through the medium. A cascade of secondary electrons is created in this way. Electrons induced by swift ions are often called "delta-rays", and the zone of high ionization density close to the ion trajectory is referred to as "track core". The detailed knowledge of the microscopic structure of ion tracks is necessary for understanding radiation effects in condensed matter such as track formation, radiolysis, relative biological effectiveness (RBE) calculations for hadron-therapy to name a few. In these examples, doubly differential electron ejection cross sections are a key input parameter for numerical simulations (Spohr, 1990; Kraft, 2000). Useful books containing comprehensive reviews on electron emission from solids include Devooght et al. (1991) for theoretical aspects, Hasselkamp et al. (1991) for experimental aspects and Baragiola (1993). Electron ejection in single collisions (gas targets, primary ionization) was treated by Stolterfoht et al. (1997). A large number of reviews in common journals are also available.

Important parameters which can be varied in experiments or calculations are first of all the properties of the projectile such as its velocity v_P, atomic number Z_P or charge q_P, and the number n of constituents in the case of cluster projectiles. In the following, we exclude "molecular (cluster) effects" and refer the reader to

the review by Fallavier (1996). Also, we restrict our discussion to the high velocity regime (electronic stopping) and exclude effects related to elastic ("nuclear") stopping or effects related to the potential energy (see the contribution by Winter et al. in this book for information about electron emission in the low velocity regime). The impact angle δ between the beam and the target surface normal may range from $\delta = 0°$ (perpendicular incidence) to δ close to 90° (grazing incidence). Basic properties of the target are its atomic number Z_T (keeping in mind that many materials are made of atoms of different kinds) and the thickness d. The target surface has a great influence on low energy electron emission (structure, topography, surface impurities due to physisorption and chemisorption). Furthermore, effects related to the orientation of either incoming beam or outgoing electrons with respect to a crystal direction (channeling, etc.) or the target temperature (surface modification, phase transitions) may arise.

Electron emission from solid surfaces under electron and ion impact was first observed at the end of the 19th century along with all the major discoveries concerning cathode rays, canal rays and radioactivity. The first systematic studies were performed by Füchtbauer (1906a, 1906b) exactly one hundred years ago. In his quite remarkable papers, Füchtbauer (1906a, 1906b) already described most of the basic features concerning electron yields, angular distributions and even velocity distributions. Nowadays, electron emission from solids is fairly well understood. Generally, a three step process is assumed: (1) primary ionization (both of target and projectile), (2) transport (elastic scattering, inelastic processes, secondary electron cascade multiplication), (3) transmission through the surface potential barrier. We should keep in mind that we are dealing with a complex phenomenon (many particles, target properties, surface phenomena). Theoretically, the phenomenon can be described at different levels of sophistication. A basic description is provided by the semi-empirical theory based on the classical paper by Sternglass (1957) with possible extensions for forward and backward emission from thin foil targets (Jung et al., 1996).

All theoretical approaches are based on master phase space equations. Most of them require first the knowledge of ion-solid interaction cross sections to model the primary excitation which gives rise to secondary electron cascades. They also need electron transport cross sections to account for electron transport and escape from the solid. These cross section are not easy to calculate and at the simplest level of modeling, they are eliminated to the benefits of empirical parameters like stopping power and transport or escape length (Sternglass, 1957). More involved models make an attempt to introduce explicitly the cross section in the master equation. Various approximations have been used to determine them. They are usually deduced from first order perturbation theory (see, e.g., Beuve et al., 2002,

and references therein) at various levels of sophistication to account for solid state effects. We can distinguish three approaches: (1) approximations which neglect the electronic structure of the target and where transport is considered as a series of atomic collisions (Schou, 1980; Schiwietz et al., 1990), (2) models based on jellium theory which are able to account for collective effects like plasmon excitation (Devooght et al., 1987; Dubus et al., 1993; Juaristi et al., 1998), and (3) models where the electronic structure is taken into account explicitly (Willis et al., 1974; Chung and Everhart, 1977; Rösler and Brauer, 1981, 1988) or empirically (Beuve et al., 2002). The master phase space equation has been solved by direct integration in the case of stationary flux approximation (Schou, 1980; Devooght et al., 1987; Rösler and Brauer, 1981, 1988) or by Monte Carlo simulation (Lencinas et al. 1990, Dubus et al. 1993, Beuve et al. 2002). The latter method provides more freedom regarding the geometry and interaction with the surfaces of the target. The calculated (total and differential) electron yields are in good qualitative agreement with experiments and allow interpretation of many experimentally observed features.

2. Experimental Techniques: New Developments

Experimentally, doubly differential electron yields (in single collisions with gas targets, doubly differential cross sections) are recorded with the help of both magnetic or electrostatic spectrometers, and time-of-flight techniques. The spectrometer is placed at a certain observation angle θ, and the doubly differential electron yields, i.e. energy or momentum spectra, are measured by varying the electric or magnetic field of the analyzer. The ejection angle θ is usually measured with respect to the beam direction, i.e. $\theta = 0$ deg. denotes emission in the direction of the beam. Secondary electron yields (the mean number of electrons emitted per projectile) can be obtained from current measurements or from the measurement of electron emission statistics, i.e. the probability $P(n)$ that $0, 1, 2, \ldots, n$ electrons are emitted. More details on experimental techniques can be found in e.g. Hasselkamp et al. (1991) and Stolterfoht et al. (1997). During the last 10 years, important new experimental techniques were applied to electron ejection. Advanced electrostatic spectrometers (toroidal geometry of the deflection plates; see Bechthold et al., 1998) allow to simultaneously measuring the complete electron angular distribution at given electron energy with good angular resolution. This feature allowed to identify never before seen spike-like narrow electron jets along the beam axis in electron emission from thin foils, which may possibly be due to a plasma-lens (track guiding) effect (Zäpfel et al., 2002).

The multi-detector ARGOS, initially designed for studying nuclear reaction products, was adapted for the measurement of fast electrons (Lanzanò et al., 1998; De Filippo et al., 2004). With this multi-detector, in comparison to conventional spectroscopic methods used in atomic collisions up to now, three important advantages are achieved: (1) doubly differential velocity spectra can be measured simultaneously at many ejection angles (up to 120 detectors), (2) absolute ejection yields and cross sections can be measured with great accuracy thus allowing a stringent test of ionization theory, and (3) (multi-) coincidences can be measured. This latter feature opens the door for studies of processes which have not yet been accessible, e.g. correlated emission of two or more electrons. Such studies become also feasible for low energy electrons via the measurement of the time-of-flight of electrons combined with imaging techniques (derived from the "reaction microscope", see e.g. Ullrich et al., 2003), a technique that has been successfully applied to study particle ejection in ion-atom and ion-molecule collisions. A combination of electric and magnetic fields guide the ejected electrons onto a position sensitive detector. The full differential emission characteristics of up to 10 electrons per single incoming ion can be extracted (Rothard et al., 2007).

3. Overview: Basic Mechanisms

Basic mechanisms of electron ejection such as primary ionization in binary encounter collisions, multiple collision sequences, electrons transport and collective excitation (wake, plasmons) are summarized in Figure 1 and explained in more detail throughout the text. Primary ionization in close collisions leads to ejection of fast (δ-) electrons from the target atoms (binary encounter, denoted P in Figure 1). Low energy electrons stem from ionization in distant collisions or from collective effects such as plasmon decay or directed emission of shock electrons from the ion-induced wake. On their way through the solid towards the surface, electrons suffer inelastic collisions or angular scattering (electron transport). The projectile can be ionized (electron loss, denoted T in Figure 1). Higher order collision sequences (P-T-P-..., referred to as "Fermi shuttle") may also occur. Figures 2 and 3 show examples of doubly differential spectra of low energy ($E < 3$ keV) electrons in backward and forward direction (Figure 2) and of high energy electrons ($E > 10$ keV) in forward direction (Figure 3).

A prominent feature in these latter spectra are "binary encounter electrons" with a broad distribution around a velocity of $v_{\mathrm{BE}} = 2v_{\mathrm{P}} \cos\theta$. Another feature are "convoy electrons" (CE) from either electron loss or capture to low-lying projectile continuum states. The paper by Breinig et al. (1982) still is an excellent introduction to CE. Their energy is close to zero in the projectile frame, and they

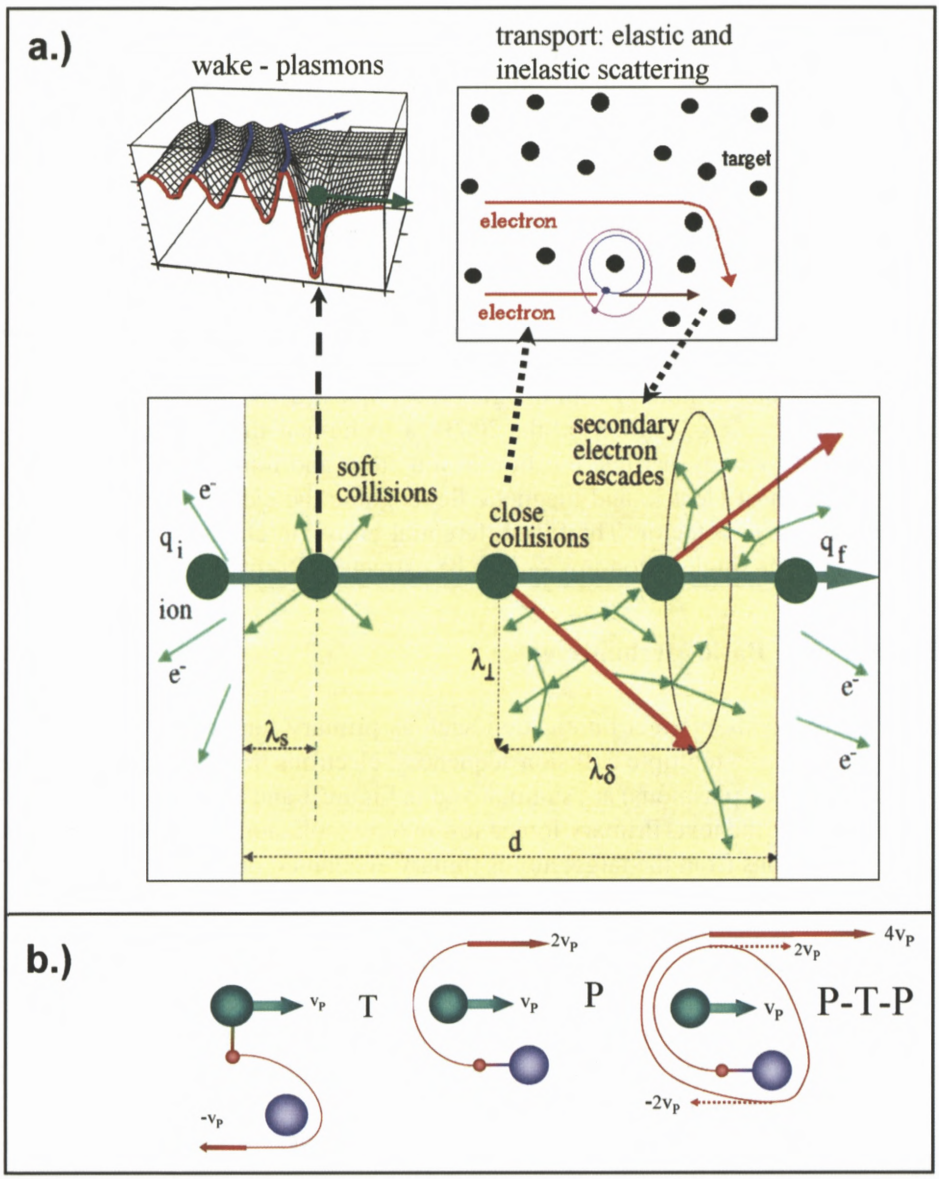

Figure 1. (a) Basic mechanisms of electron ejection from a thin foil of thickness d bombarded with an ion beam of incoming charge q_i and outgoing charge q_f. Low energy electrons stem from ionization in distant collisions or collective effects (plasmon decay and wake, upper left part). Primary ionization in close collisions leads to ejection of fast (δ-) electrons from the target atoms. On their way through the solid towards the surface, electrons suffer inelastic collisions without angular deflection or angular scattering (upper right part) and may create secondary electron cascades. (b) Target ionization by a binary encounter projectile-electron collision (P), projectile ionization by the target (electron loss, T) and higher order collision sequences (Fermi shuttle P-T-P-...).

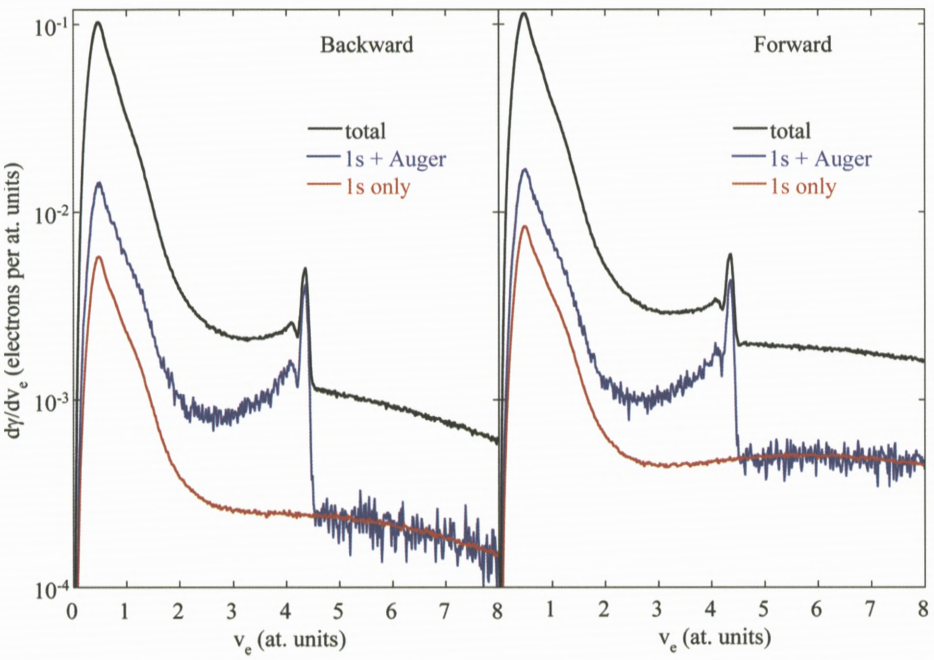

Figure 2. Low energy electron spectra) for H^+ (9 MeV/u) penetrating a thin carbon foil (4 μg/cm^2) in backward (beam entrance side, left) and forward (beam exit side, right) direction. The numerical simulation (Beuve et al., 2002) is based on the Monte Carlo method, therefore, statistical fluctuations naturally arise and can be seen in the spectra. Shown are the total velocity differential spectra, the contribution of the K-shell 1s ionization, and the contribution of KLL Auger electron emission. The most prominent feature is the peak of low energy often so-called "secondary electrons" at typically a few eV which stem from both primary ionization and cascade multiplication. Also, a shoulder from the decay of volume plasmons (at $E < 20$ eV for C targets) is visible.

form a characteristic cusp shaped peak in fast forward electron spectra. Recently, absolute cross sections for convoy electron emission from thin foils in a wide range of Z_T (C ... Bi) by fast projectiles (23–95 MeV/u) were measured with the ARGOS multi-detector (De Filippo et al., 2004). A numerical description of convoy electron transport through solids in the vicinity of the projectile Coulomb field was developed by Burgdörfer and Gibbons (1990). Note that the production of CE in low lying projectile continuum states, the population of highly excited bound (Rydberg-) states of (heavy) ions in solids and the evolution of the ion charge states are related. A further electron ejection mechanism is the Auger effect. Projectile Auger electrons from in-flight de-excitation of heavy ions carrying electrons in bound excited states can be observed (Figure 3). A review on this

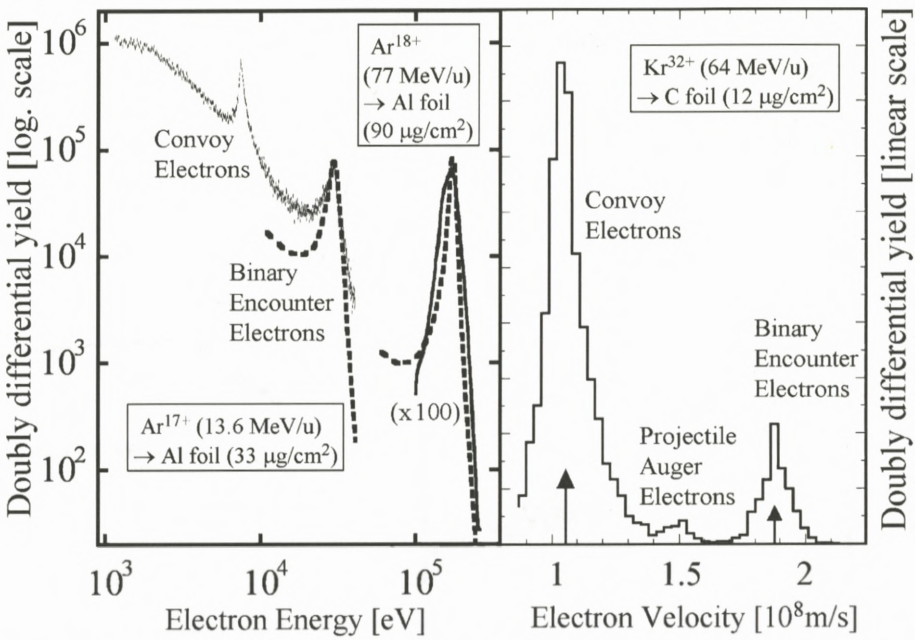

Figure 3. Fast-electron spectra emitted in forward direction (beam exit side, near $\theta = 5$ deg.) from thin foils, showing convoy- and binary encounter electrons. Left-hand side: doubly differential electron yields $d^2\sigma/(dE\, d\Omega)$ plotted as a function of the electron energy for the collision system Ar on Al foil. Comparison of experimental spectra at 13.6 MeV/u (thickness 33 μg/cm^2, Rothard et al., 1998) and at 77 MeV/u (thickness 90 μg/cm^2, Lanzanò et al., 1998) to the EIA calculation (dotted lines). In this latter case, the left-hand scale corresponds to units of barn/(keV sr). Right-hand side: Forward electron velocity spectrum induced by Kr^{32+} (64 MeV/u) from a C foil of approx. 50 nm (experimental data). Note the projectile Auger electrons.

topic was given by Stolterfoth (1987). Target Auger electrons (typically at low energies $E < 3$ keV) appear in the low energy electron spectra (Figure 2).

The low energy electron spectra from a calculation according to Beuve et al. (2001, 2002) for H^+ (9 MeV/u) penetrating a thin carbon foil (4 μg/cm^2) in backward and forward direction (Figure 2) show as most prominent feature the peak of often so-called "secondary electrons" at typically a few eV. This broad distribution stems from both primary ionization and cascade multiplication (secondary electrons). Also, a shoulder from the decay of volume plasmons (at $E < 20$ eV for C targets) is visible. An interesting feature of theoretical calculations is that different contributions to electron ejection can be separated. Therefore, in Figure 2, we show the total velocity differential spectra in comparison to the contribution of the K-shell 1s ionization and the contribution of KLL Auger electron emission.

The overall intensity is slightly higher for forward emission. Experimental data may also serve as a benchmark for the development of numerical simulations of electronic energy deposition in matter and electron emission. After this rapid overview, we now discuss some special topics in more detail. We do not attempt at an exhaustive review, but rather would like to highlight the most important basic features, recent important new developments and findings, and open questions.

4. Primary Ionization, Fast Electron Transport and Collision Sequences

A "binary encounter" (BE) collision between projectile and target electron leads to ejection of electrons with a velocity of $v_{\mathrm{BE}} = 2v_{\mathrm{P}} \cos\theta$ if the interaction with the target nucleus is neglected. The momentum $p = \gamma v$ with $\gamma = (1-(v/c)^2)^{-1/2}$ is the relevant quantity (instead of v_p) for relativistic projeciles. The observed BE electron peak shows a broadening due to the initial momentum distribution of the bound target electrons known as Compton profile (Figure 3). The BE process is theoretically well understood. The relativistic theory is based on the electron impact approximation (EIA), where ionization takes place via electron transfer to the projectile continuum in a quasi-elastic scattering of the target electron by the projectile Coulomb field (Jakubassa-Amundsen, 1997; see also Rothard et al., 1998a). The corresponding cross section is then folded with the Compton profile in the initial state.

Measurements of electron spectra as a function of the target thickness allowed observing how electron emission evolves from single collisions (as in atomic collisions with low density gas targets) up to multiple collisions (as in the bulk of solids, where electron transport phenomena become important) and thus to link single collisions to effects in condensed matter. A transport theory, based on the "Separation of Energy Loss and Angular Straggling" approximation (Tougaard and Sigmund, 1982; Schiwietz et al., 1990), was developed. It was tested for different collision systems (13.6 MeV/u and 95 MeV/u Ar^{18+} GANIL, and 45 MeV/u Ni^{28+}, LNS Catania) (Rothard et al., 2001; De Filippo et al., 2004). Singly differential cross sections, which vary with ejection angle θ as $\mathrm{SDCS}(\theta) \sim \cos^{-3}\theta$, obtained from measurement and calculation agree within some percent for thin foils, and so do doubly differential electron yields (as can be seen in Figure 3, left-hand side). The evolution of the shape of the spectra is reasonably well reproduced. Another important result concerns the target material dependence of BE electrons. It was found experimentally that they roughly follow a very simple scaling law: the BE electron yield is proportional to the number of target electrons "seen" by the projectile (Bechthold et al., 1998; Rothard et al., 1998a; De Filippo et al., 2004).

Another interesting result is the observation of unexpectedly high cross sections for electron emission at energies far beyond the BE peak, at large angles and even in backward direction. Possibly, this can be explained by the so-called "Fermi-shuttle" process, which was introduced to explain the origin of high-energy cosmic radiation due to acceleration of charged particles by repeated collisions with moving magnetic fields in interstellar space. Evidence for such acceleration schemes were found in ion-solid collisions (Lanzanò et al., 1999) and ion-atom collisions (Sulik et al., 2002). From the basic BE process (ionization of the target by the projectile, P) and its counterpart in the projectile frame (T, ionization of the projectile by the target: electron loss), collision sequences (consecutive scattering events on the target nucleus and the projectile nucleus) can build up such as e.g. P-T, P-T-P, T-P, etc. as shown schematically in Figure 1b. It was shown that the Fermi shuttle electron yield increases with the perturbation parameter Z_P/v_P, and also with the more realistic scaling parameter $Z_P^2 Z_T/6v_P^3$, which takes into account re-bouncing of the electrons on target and projectile. This finding points towards the important role of the combined projectile-target system (Rothard et al., 2005).

The velocity distribution $N(v)$ of the fast Fermi shuttle electrons is exponentially decreasing, i.e. $N(v) \sim \exp(-nv)$, and exhibits the same evolution of n with projectile velocity as in the case of Fermi accelerated target deuterons. The Fermi shuttle acceleration should become of particular importance in ion-solid collisions compared to ion-atom collisions, because of the high target nucleus density. In this case, there should be an enhanced probability of re-scattering of electrons all along the projectile trajectory, since the projectile sees the projected density of backscattered electrons along the ion track. But this is an open question, since a direct comparison of data from thin foils and gas targets is still missing. Furthermore, when heavy collision partners (heavy target atoms, heavy ions) are involved, the re-scattering probability increases. This may have consequences for the microscopic structure of ion tracks (micro-dosimetry) and radiation induced energy deposition in both inert and living matter. We note that collision sequences of orders higher than P-T-P were observed (Sulik et al., 2003). A further problem to be solved lies in quantification of the absolute contribution of such Fermi shuttle processes to electron ejection yields and to radiation effects. Monte Carlo simulations are useful in this respect (Sulik et al., 2003).

As far as primary ionization is concerned, an important recent theoretical development is the application of the binary stopping theory in a straightforward way to calculate ejected electron spectra (Weng et al., 2006). In this treatment, the contributions of target and projectile ionization are included. From an experimental point of view, the application of the "reaction microscope" to electron emission

in primary ionization allowed in particular studying the low energy part of the spectra down to less than eV energies (Ullrich et al., 2003). In the low electron energy limit (soft collisions with low momentum transfer), the influence of the target nucleus increases (two center effects). Also, for a realistic description of soft electron emission, quantum mechanical treatments are necessary. The emission of low energy electrons is governed by dipole transitions. For example, for a simple hydrogen target, most low energy electrons are emitted around $\theta = 90$ deg., i.e. $\cos\theta = 0$. Nevertheless, the Compton profile, the initial momentum distribution of the bound electrons, broadens the distribution and leads to emission towards all angles. For complex targets (molecules with many electrons), the angular dependence is much weaker than for hydrogen, and smeared out over all angles.

5. Low Energy Electrons: Collective Excitations

Low energy electron emission (below 1 keV) strongly depends on surface properties, and bears features of collective excitation (plasmons, wake), of transport effects (cascade multiplication, low energy "secondary" electron peak, Figure 2) and of effects connected to strong perturbation ("high charge effects", see below, Figure 6). Plasmon excitation and subsequent electron emission following plasmon decay is well known (see Figure 2) and well treated theoretically in particular for Al. Collective plasmon-like excitations were also observed for Be, C, Mg, Si, Ti, Nb and Au (Hasselkamp et al., 1991). Low energy electron emission from metals in backward direction was intensively studied by the Giessen group (Hasselkamp et al., 1990).

The collective response of the ensemble of target electrons to a moving charge shows up as electron density fluctuation with a Mach cone-like spatial structure (Echenique et al., 1979). This so-called "wake" is related to plasmon excitation, and may lead to a directed emission of low energy electrons perpendicular to the shock front as shown in Figure 1 (top left part). For theoretical treatments see Schäfer et al. (1980) and Brice and Sigmund (1980), the first experiment with controlled surfaces was performed by Burkhard et al. (1987b). An open problem here is the coupling to the surface and the de-excitation from a collective state inside the solid to a single electron continuum state outside the solid (Griepenkerl et al., 1995). A search for the possible influence of a superconducting phase transition on collective electron emission (Rothard et al., 1992) was performed but did not reveal an important dependence of electron emission characteristics on the target temperature above and below the transition temperature.

Another phenomenon was searched for: the existence of bound states of electrons in the wake of ions inside the solid and the possible trapping of electrons

as suggested by Neelavathi et al. (1974). Experimental searches for such "wake-riding" electrons in connection with experimental studies of the convoy electron peak remained without success. However, the wake of negatively charged particles heavier than electrons may lead to an enhanced probability of single electron trapping in wake-bound states (Burgdörfer et al., 1989). Experimental investigations by Yamazaki et al. (1990) showed evidence for an additional "wake" related mechanism for electron emission in forward electron spectra induced by antiprotons passing through thin carbon foils. Interestingly, in contrast to the case of positively charged particles, there is no convoy electron peak at $v_e \approx v_P$ with negatively charged projectiles, but an "anticusp" caused by the repulsive interaction between the antiproton and the electrons. However, the anti-cusp is filled up by scattered electrons in the case of solid foils.

6. Electron Yields: Scaling Laws

During the ION06 meeting, it became clear that there is interest in knowing the behaviour of electron emission and to find simple scaling laws as a function of v_P, Z_P and target thickness d for applications. First of all, since very often thin foils are used as electron source for e.g. beam monitors and dosimetry, let us have a look at the target thickness dependence of electron emission. Forward and backward electron yields are plotted as a function of the target thickness in Figure 4 for Cu ions of 9.6 MeV/u, and for Ni ions of 74 MeV/u. These experiments are based on current measurements as described by e.g. Clouvas et al. (1997) and Beuve et al. (2001). Also, yields for proton impact at 0.5 MeV/u and 9 MeV/u, calculated by means of a numerical simulation based on the Monte Carlo method, are shown (Beuve et al., 2001). Forward yields γ_F evolve over a large target thickness range and finally reach a plateau $\gamma_F(\infty)$. This is related to cascade multiplication by high energy δ-electrons which are mainly emitted in the forward direction. Backward yields rapidly reach a saturation value $\gamma_B(\infty)$ except at 74 MeV/u, where a second plateau is observed. In the case of forward electron yields, one must be careful and take into account that the ions loose energy in the foil. Their energy upon exit $E_P - \Delta E_P$ may considerably differ from the initial energy E_P upon entrance. The energy loss ΔE_P increases with target thickness. At high projectile energies, forward electron yields are "in equilibrium" (Figure 4) for foils thin enough to ensure that the energy loss is small compared to the initial energy $\Delta E_P \ll E_P$. However, such effects may become important at energies below the stopping power maximum (Clouvas et al., 1997; Beuve et al., 2001).

Electron transport can be studied by an analysis of measured electron yields as a function of foil thickness within the framework of an empirical theory (Stern-

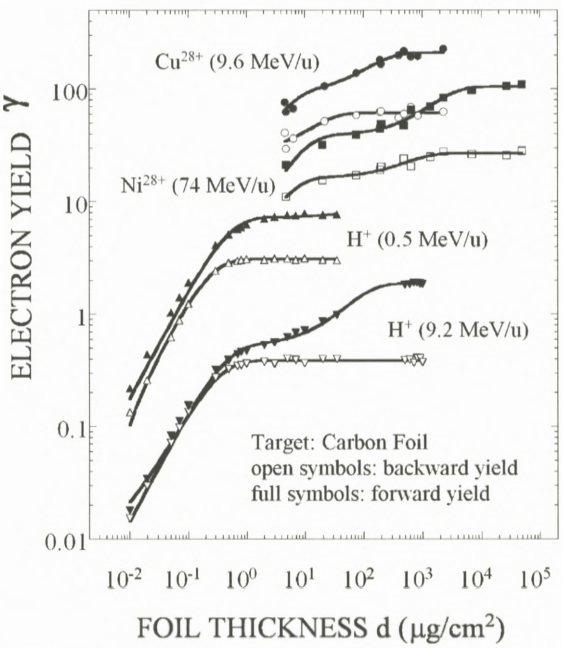

Figure 4. Forward (full symbols) and backward (open symbols) electron yields (γ_F, γ_B) as a function of carbon target thickness d. The lines drawn through the experimental data are fits of Equation (1) to γ_F and with Equation (2) to γ_B. A thickness of $d = 1$ μg/cm^2 corresponds to about 61 Å for a carbon foil density of $\rho = 1.65$ g/cm^3. Projectiles: Cu^{28+} (9.6 MeV/u, circles, experiment, Jung et al., 1996), Ni^{28+} (74 MeV/u, squares, experiment, Jung et al., 1996), H^+ (0.5 MeV/u, triangles, numerical simulation, Beuve et al., 2002), H^+ (9.2 MeV/u, upside-down triangles, numerical simulation, Beuve et al., 2002).

glass, 1957; Jung et al., 1996). The following equations are deduced for the target thickness (d) dependent forward (γ_F) and backward (γ_B) low energy electron yields:

$$\gamma_F(d) = \Lambda_F \frac{dE}{dx}\left(1 - \beta_S\, e^{-d/\lambda_S} - \beta_\delta\, e^{-d/\lambda_\delta}\right), \tag{1}$$

$$\gamma_B(d) = \Lambda_B \frac{dE}{dx}\left(1 - F_1\, e^{-d/\lambda_S} - F_2\, e^{-d/\lambda'_\delta}\right). \tag{2}$$

Here, Λ_F and Λ_B are constants and dE/dx is the electronic energy loss per unit path length. The curves shown in Figure 4 are fits with Equation (1) to the forward yields and with Equation (2) to the backward yields. The evolution of both theoretical and experimental data with target thickness is remarkably well reproduced

by these simple formulae. By means of this fitting procedure, one can deduce the mean *diffusion length for slow electrons* λ_S and the mean *transport (attenuation) length* for high energy electrons (in forward direction: λ_δ, in backward direction for backscattered fast electrons: λ'_δ). The meaning of these quantities is shown schematically in Figure 1 (central part). One also can deduce the "partition factor" β_δ, which measures the fraction of projectile energy lost in close collisions with subsequent high energy δ electron emission. The fraction dissipated in soft collisions, leading to direct production of low energy electrons or to plasmon excitation with subsequent plasmon decay, is given by $\beta_S = (1 - \beta_\delta)$. Under the assumption that $\lambda_S \ll \lambda'_\delta \ll \lambda_\delta$, it can be shown that

$$F_1 = 1 - F_2,$$

$$F_2 = -\beta_\delta \lambda'^2_\delta (\lambda_\delta + \lambda'_\delta + \beta_\delta \lambda_\delta)^{-1} (\lambda_S - \lambda'_\delta)^{-1},$$

see Jung et al. (1996).

The low energy electron diffusion length λ_S does not depend on the ion species or projectile energy and is of the order of 30 Å for carbon, whereas λ_δ increases strongly with increasing projectile velocity. This explains the "velocity effect" where different damage in solids occurs at the same electronic energy loss dE/dx, but at different ion velocities. The energy having been taken away from the track core by fast electrons increases with ion velocity for faster ions. This leads to a reduced density of energy deposition close to the ion track. Such a velocity effect was also observed in ion induced electron emission by Neugebauer et al. (1999). Due to the high projectile velocity, it is possible to clearly distinguish λ_S, λ'_δ and λ_δ at 74 MeV/u, but not around 10 MeV/u, where both exponential functions of Equation (2) merge and the backward yield increase can be described by one single exponential function.

The partition factor β_δ does not depend significantly on the ion energy, but rather increases strongly with Z_P from 0.35 with protons up to 0.75 with Ni/Cu. This finding is related to so-called "saturation effects" (see below, discussion of high charge effects, Figure 6), since for heavy ions, the proportion of low energy electron emission in primary ionization (from soft collisions with large impact parameter) decreases with Z_P compared to high energy electron emission (from violent collisions at small impact parameters). This leads to reduced electron emission in backward direction and enhanced emission in forward direction. Indeed, the ratio of forward to backward yields $R = \gamma_F/\gamma_B$ for "thick" targets strongly increases with projectile atomic number from approx. $R = 1.2$ for protons up to $R = 5$ for the heaviest ions.

Coming back to relevant scaling, the electronic energy loss per unit path length dE/dx immediately comes into mind as a first choice of an appropriate scaling

parameter. Such a proportionality is indeed suggested in several theoretical approaches (Sternglass, 1957; Sigmund and Tougaard, 1981). To test this hypothesis, we can compare electron yields to $\mathrm{d}E/\mathrm{d}x$ by defining a ratio

$$\Lambda_i(Z_\mathrm{P}, v_\mathrm{P}) = \frac{\gamma_i}{\mathrm{d}E/\mathrm{d}x} \,. \tag{3}$$

The index i stands for B, F or T if backward (from the beam entrance side), forward (the beam exit side in the case of thin foils), or total electron yields are concerned ($\gamma_\mathrm{T} = \gamma_\mathrm{F} + \gamma_\mathrm{B}$). In practice, rather $\mathrm{d}E/\mathrm{d}(\rho x)$ measured in keV/(μg/cm^2) than $\mathrm{d}E/\mathrm{d}x$ is used and tabulated. The parameter Λ is often called "material parameter" in the literature and it is assumed that it depends on the target material only. This is wrong, as we will see in the following, since it also depends on the projectile parameters v_P and Z_P. It should be kept in mind that, if the condition $\Delta E_\mathrm{P} \ll E_\mathrm{P}$ is not fulfilled, ΔE_P may lead to a different $\mathrm{d}E/\mathrm{d}x$ at the beam exit side. This should be taken into account when calculating Λ_F with Equation (3) (Beuve et al., 2001).

The dependence of the ratios Equation (3) for protons, carbon ions, nickel (copper) ions and uranium ions is shown in Figure 5. The foils are thick enough to assure that the plateaus $\gamma_\mathrm{F}(\infty)$ and $\gamma_\mathrm{B}(\infty)$ are reached. In all cases, an increase of Λ_i is observed. It is more pronounced the heavier the ion, and stronger for forward than for backward yields. Note that Λ values are different above and below the electronic stopping power maximum (see above, velocity effect, Neugebauer et al., 1999). Finally, we mention that a simple empirical law for the charge dependence of backward emission was proposed by Beuve et al. (2000):

$$\Lambda_\mathrm{B}(q_\mathrm{P}) = \Lambda_\mathrm{B}(q_\mathrm{P} = 1)\left(2 - q_\mathrm{P}^2 \frac{\mathrm{d}E/\mathrm{d}x(q_\mathrm{P} = 1)}{\mathrm{d}E/\mathrm{d}x(q_\mathrm{P})}\right). \tag{4}$$

If low energy electron energy distributions (singly or doubly differential yields) are needed, the above scaling of the integrated forward and backward emission yields (Jung et al., 1996; Rothard et al., 1998b; Beuve et al., 2000, 2001) can be combined with doubly differential low energy electron spectra for fast proton impact as measured by Drexler and Dubois (1996).

7. Strong Perturbation: High Charge Effects

Several specific effects connected to the high projectile charge of swift heavy ions in electron emission were observed. Examples are the saturation of low energy electron yields, appearance of hypersatellite lines due to multiple ionization of inner shells and a broadening of Auger lines (see e.g. Rothard, 2004; Schiwietz

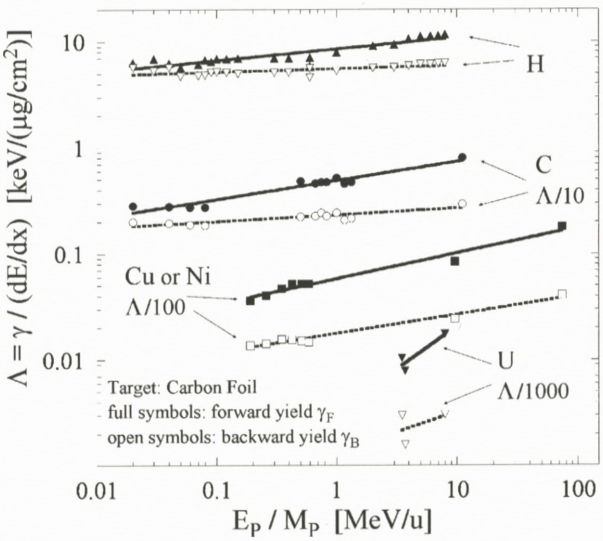

Figure 5. The ratios of forward electron yields (full symbols) and backward yields (open symbols) to the (electronic) energy loss per unit path length (Equation 3) as a function of the projectile energy divided by ion mass, E_P/M_P, for protons (triangles), carbon (circles), nickel/copper (squares) and uranium ions (upside-down triangles). The Λ-values were divided by the indicated factors. The lines are fits of a power law $\Lambda = C(E_P/M_P)^n$ to the data (similar plots shown in Rothard et al., 1998, here revisited and enriched with new data where available). The target thickness was chosen so that electron yields have reached the (projectile velocity dependent) asymptotic equilibrium value (see Figure 4, typically 500 μg/cm^2 at 10 MeV/u). The charge state of the incoming ions is close to the mean final charge.

et al., 2004, and references therein). Important results on high charge effects were obtained from measurements and theoretical calculations of low energy electron spectra. In ionization theory, the ratio q/v_P of charge and projectile velocity measures the strength of perturbation induced by the projectile (see e.g. Stolterfoth et al., 1997; Beuve et al., 2002). We can vary this parameter in a straightforward way by performing experiments with projectiles of different charge or atomic number while keeping the projectile velocity constant. In order to avoid effects connected to charge exchange or screening, it is important to do the experiments aimed at exploring the influence of the perturbation parameter with ions of charge states close to the mean equilibrium charge. The role of projectile electrons (active and passive screening) was e.g. discussed by Clouvas et al. (1997).

In Figure 6, the ratios of backward electron energy spectra obtained with Mo^{39+} and spectra obtained with C^{6+} (at constant projectile velocity of 9.2 MeV/u, about 19 atomic velocity units) are shown. Here, the perturbation

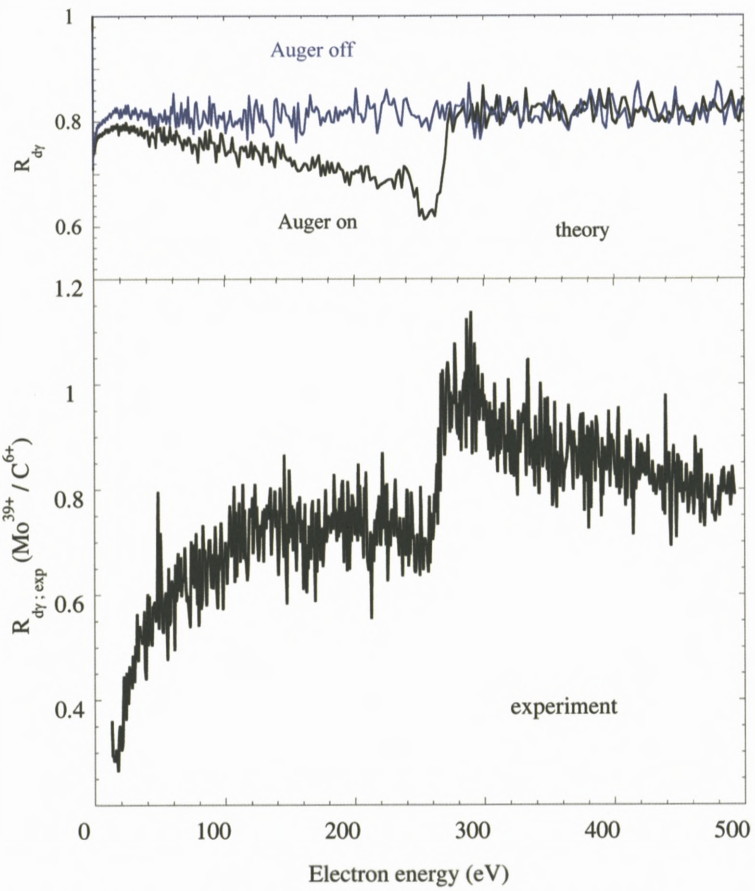

Figure 6. The ratios of backward electron energy spectra obtained with Mo^{39+} and spectra obtained with C^{6+} (at constant projectile velocity of 9.2 MeV/u, about 19 atomic velocity units) on carbon. The differential emission yields are divided by q_P^2. Top: numerical simulation (Beuve et al., 2002) including the carbon KLL Auger emission ("on") and without carbon KLL Auger ("off"). The numerical simulation is based on the Monte Carlo method, therefore, statistical fluctuations naturally arise and can be seen in the spectra. Bottom: experiment (Caron et al., 2001).

strength (given in atomic units) was varied from $q/v_P = 0.065$ (weak perturbation) to $q/v_P = 2$ (strong perturbation). The differential emission yields were divided by q_P^2, since in first-order theory one would expect such a q_P^2 scaling. If no high charge effects were present, the ratio should be constant and equal to one. This is not observed: the shape of these ratios varies with energy, and thus electron spectra depend on q_P. At large electron energy, a q_P^2 scaling law is observed: the

ratios, divided by q_P^2, are approximately equal to unity within the experimental uncertainty. In contrast, at lower energy (below the 1s ionization threshold) a strong deviation from a simple q_P^2 scaling occurs. This high charge effect (reduction of low energy electron yields with respect to a q_P^2 scaling) saturates with increasing q_P: the ratios of low energy electron yields divided by q_P^2 decrease with q_P and approach a constant saturation value.

The experimental results thus show a "reduction effect" with respect to a q_P^2 scaling for low energy electron emission under strong perturbation by heavy projectiles. Such an effect is mainly connected to low energy electron emission, below the K-shell ionization threshold (carbon KLL Auger electron emission, see Figures 2 and 6). In Figure 6, both calculation (top) and experimental data (bottom) are shown. The numerical simulations allow studying the influence of the contribution of carbon KLL Auger electron emission ("Auger on/off"). An important result is that the experimentally observed variation of the ratios can only be qualitatively reproduced by theory if Auger emission is taken into account.

In the present case of high projectile velocities, the saturation cannot be explained in terms of screening of the projectile's charge by polarized target electrons for distant collisions as suggested by Koyama et al. (1986). Reduction effects could rather arise from either (1) specific high charge effects in primary ionization, or (2) collective effects on electron transport in the vicinity of the projectile (Borovsky and Suszcynski, 1991; Benka et al., 1995). The ion creates a positively charged zone in its wake, leading to an attractive track potential which results in an attractive force on the electrons moving away from the ion track. Recent theoretical investigations rather point towards "saturation effects" of ionization cross sections with increasing ion charge (Beuve et al., 2002). This model going beyond first order theory by using a distorted wave approach (CDW-EIS) for the primary ionization allows reproducing qualitatively (but not yet quantitatively) the electron yield reductions (Figure 6). The model takes into account two-center effects (the electron moves in the combined fields of projectile and target nuclei) and can be further amended by taking into account multi-electron effects (Gervais et al., 2003). In particular, modification of the binding energies occurs. This is caused by multiple ionization, a specific feature observed with heavy ions. It can directly be observed in electron spectra, where complete K-shell ionization leads to the appearance of Auger hypersatellite lines.

8. Auger Electrons: Electronic Temperatures

It was observed that ion induced Auger electron lines become broader with increasing projectile charge. Schiwietz et al. (1999) suggested that this broadening

of Auger lines could be due to increasing "electronic temperatures" of valence electrons. The width of the Auger lines is connected to the energy width of the occupied density of states at the time of the Auger decay. It is possible to deduce the mean "electronic temperature" of the target for the corresponding Auger decay time (typically about 10 fs for carbon) from the primary Auger spectra, taking into account instrumental resolution and slowing down of Auger electrons during their transport to the surface by means of a numerical simulation. The "background" consisting of ionization electrons (continuous decrease) and possibly hypersatellite lines is subtracted. The total electron energy distribution $n(\varepsilon, T) = D(\varepsilon) f(\varepsilon, T)$ of the valence electrons is obtained from the convolution of the temperature-dependent Fermi distribution $f(\varepsilon, T)$ and the calculated band structure (density of states) $D(\varepsilon)$. Finally, one can adjust the temperature T of the Fermi–Dirac distribution $f(\varepsilon, T)$ so that the total width (not the FWHM) of the calculated electron energy distribution $n(\varepsilon)$ best fits the measured width of the primary Auger spectrum. This procedure, applied by Caron et al. (2001, 2006), differs from the one used by Schiwietz et al. (1999, 2000), the latter one being based on a comparison to electron induced spectra and fitting of calculated spectra (with temperature T as only free parameter) to the slope of the high-energy side of measured spectra.

The energy width of the primary Auger ΔE spectra increases as a function of the projectile charge: at 9.2 MeV/u, for example, $\Delta E = 42$ eV with C^{6+} and $\Delta E = 50$ eV with Ni^{27+}. In this case, the best fit of the width is obtained at two different temperatures of $T = 11600$ K and $T = 24000$ K, for C and Ni impact, respectively. The measured temperature values can now be compared to the predictions of "thermal spike" numerical simulations. The calculations reproduce the evolution of the temperature with projectile charge, but, depending on the model, may underestimate the temperatures by up to a factor of three. We refer the reader to Schiwietz et al. (2000) and Caron et al. (2006) for detailed discussions of the corresponding thermal spike models and comparison to experiment. The spectroscopy of ion-induced Auger electrons is an experimental method to obtain quantitative information about the onset of the thermal spike. Information about the "track temperature" at later times and its evolution may be accessible via the measurement of the velocity of sputtered and desorbed particles from the surface. We finally note that his method was mainly applied to carbon targets (see Schiwietz et al., 1999, 2000, 2004; Rothard, 2004; Caron et al., 2001, 2006). Also, heavy ion induced Auger electron spectra from other target materials such as Al, Si, Be etc. were analyzed (see Staufenbiel et al., 2005, for a recent summary), but the complexity of the spectra for materials heavier than Be or C renders the interpretation more difficult.

9. Insulators: Charging Effects

Most of the results discussed in the previous chapters were obtained for metallic (conductive) targets or with thin carbon foils. Carbon foils are available in a wide target thickness range and are more or less easy to handle, even as free standing target with sufficient surface area. Metals are also relatively easy to handle and preparation of clean surfaces in ultrahigh vacuum is possible. Therefore, target-specific characteristic features of low energy electron emission (such as plasmon decay and Auger electrons) were intensively studied with metal targets. The Z_T-dependence of electron yields is relatively weak. Also, data about fast electron ejection (convoy- and binary encounter electrons) were obtained with thin metallic foils (e.g. De Filippo et al., 2004). Main dependencies on Z_T stem from the Compton profile which is much larger for high-Z_T targets and which shows up in the width of the binary encounter electron peak, and from the Z_T-dependence of electron capture and loss, which partly determine the convoy electron yield. Also, electron transport and cascade multiplication depend on Z_T. Besides the Z_T-dependence, other target properties such as conductivity or crystalline structure may have a more important influence on electron ejection.

With insulators, a build-up of charge on the target surface occurs, which makes experiments difficult. Therefore, only few experiments were performed with high velocity ions, for example with aluminum oxide Al_2O_3 under standard vacuum conditions (Borovsky and Suszinsky, 1991). Charging has been studied widely for electron beam impact (see e.g. Cazaux, 2006, and references therein), since it is of importance for electron microscopy. Charging phenomena should be even more important for heavy ion beams, because electron yields are much higher for high-Z_P ions than in the case of electron or proton impact. As a main result, electron yields from insulators are higher than those obtained with metals of comparable atomic number. This was often interpreted in terms of a reduced work function and enhanced electron escape depth.

A few studies of electron energy spectra induced by swift (MeV/u) ions were performed. With fast protons beams, a reduction of low energy electron yields with insulators was observed by Burkhard et al. (1987a) as a function of the ion current density. These experiments were performed with amorphous hydrogen loaded (>20 at%) α-C:H targets, which are good insulators in contrast to ordinary conducting carbon foils (with a hydrogen content of typically <1 at%). Furthermore, a shift to lower energies of the convoy electron peak with increasing flux density was observed (Burkhard et al., 1987a). An energy shift of Carbon KLL Auger electrons towards lower energies with respect to Auger emission from carbon foils was observed with polypropylene foils. This was attributed to

the influence of the heavy ion nuclear track potential (Schiwietz et al., 1992). Note that in this latter case, we are dealing with a microscopic effect related to a single track, and not with a macroscopic charging effect. Measurements of particle emission with the ion flux density as parameter may be a means to distinguish between macroscopic and microscopic (track) charging. A shift of the convoy electron peak energy and a "focusing effect" of the charged ion track leading to "nuclear track guiding" of convoy electrons with polymer foils was reported by Xiao et al. (1997). In a quite recent experiment (2005) at GANIL, shifts of the convoy and the binary encounter electron peak with Kr ions at 64 MeV/u traversing mylar foils were observed.

10. Channeling and Emission Statistics

An interesting possibility to probe electron emission in relation to energy loss and charge exchange is ion channeling in crystals (see Cohen and Dauvergne, 2004, and references therein). By comparing electron emission under random impact and channeling conditions, one can study the dependence of electron production on the electron density encountered by the projectile. For well channeled ions, collisions with inner shell target electrons are strongly reduced. Therefore, the energy loss of channeled ions is only about half of that in random direction. These effects lead e.g. to a reduction of convoy electron yields (Breinig et al., 1982) and binary encounter electron ejection (Kudo, 2001). Directional effects do not only occur as far as the projectile interaction is concerned, but also have an influence on electron transport and escape from the surface (Brusilovsky, 1985).

Recently, new interest in electron emission under channeling conditions has arisen. The distribution $P(n)$ (electron emission statistics, which allows to deduce electron yields) was measured in coincidence with the energy loss $\mathrm{d}E/\mathrm{d}x$ and emerging charge states of Pb ions (29 MeV/u) after interaction of the beam with a thin Si crystal. This powerful technique allows observing correlations of forward and backward electron emission and the correlation of electron emission to a particular ion trajectory and corresponding energy loss and charge. A strong reduction of energy loss and electron emission for hyper-channeled ions (which interact mainly with target valence electrons) is observed. Furthermore, enhanced electron emission due to projectiles entering the crystal very close to atomic strings (leading to enhanced energy loss compared to random impact) occurs (Barrué et al., 2004).

The measurement of the multiplicity distribution $P(n)$ was also applied for amorphous targets without directional effects (Kozochina et al., 1993). Here, the electron emission for fixed in- and outgoing ionic charge states (Vidović et al.,

1997), the relation of electron emission and energy loss (Benka et al., 1995) and the correlation of forward and backward emission (Smidts et al., 1999) can be probed. Yamazaki et al. (1993) also measured $P(n)$ and reported a correlation of forward and backward electron emission in collisions of Ar (1.8 MeV/u) with foils as thick as 500 Å, possibly due to plasmon decay taking place all over the target thickness.

11. Other Intriguing Topics: An Open End

Let us now have a look at a choice of topics marking interesting approaches or bearing unsolved questions which therefore could be of interest as directions of future research. Further new horizons appear with experimental techniques allowing a one-ion by one-ion measurement of ejected electrons and multi particle coincidences. Examples are the reaction microscope (Ullrich et al., 2003), which was applied for studying differential multi-electron ejection from heavy ion-solid collisions (Rothard et al., 2007), and the multi-detector ARGOS (Lanzanò et al., 1998), which allows the coincident ejection of two or more electrons (Lanzanò et al., 2003). In a recent experiment, hints for an inelastic binary encounter process with simultaneous target and projectile ionization were found. This particular ionization process with a specific kinematic signature is related to so-called $(e, 2e)$ experiments allowing a stringent test of ionization theories.

Few studies exist on temperature dependence of electron emission (see e.g. Hasselkamp et al., 1991; Benka and Steinbatz, 2003). A problem here, in particular at low temperatures, is surface contamination and the relation to structural phase transitions at the surface (Benka and Steinbatz, 2004; Rothard et al., 1992). Experiments at low temperature with thin layers of frozen gases or biomolecules could be useful for radiobiology (DuBois and Drexler, 1994). Also, electron emission from insulators with microscopic and macroscopic charging phenomena will be of further interest in the future. The measurement of "electronic temperatures" via target Auger electrons from the conduction band might be a tool as probe for the femtosecond dynamics of energy deposition (Schiwietz et al., 2004). For a complete picture of energy deposition in condensed matter, however, we need to go beyond electron spectroscopy. Possibly, measurements of the velocity distribution of neutral and charged particles (secondary ions) from solid surfaces will allow to study the evolution of the "ionic temperature" of the track core at a somewhat later stage (picoseconds) depending on the electron-phonon interaction time.

Electron emission is a relatively stringent test of transport theory and modeling of specific target properties as needed in track structure calculations. However,

for strong perturbation, improved ionization theory is needed (Gervais et al., 2003). As also discussed during ION06, there is still a need for doubly differential electron emission cross sections in particular for applications in radiobiology or radiation chemistry. The microscopic dose distribution is crucial for understanding specific effects connected to light ions and heavy ions (e.g. for hadron-therapy, irradiation of polymers, radiolysis, aerospace applications) as compared to photon or high energy electron irradiation. One reason is that damage of biological tissue as well as material modification in condensed matter can be induced not only by the primary ionization of the target atoms or molecules itself, but also by secondary ionization caused by the fast δ-electrons. Even low energy electrons may be of crucial importance if such effects as electron attachment play a significant role in condensed matter. Probably, multiple ionization and possibly, inner shell Auger electron ejection may play an important role for damage induced by heavy ion beams. These topics are at the present time under vivid discussion. It is important to first study "simple" targets (atoms, small molecules) such as rare gases and then go to more complex targets (biomolecules, clusters, droplets) and finally, surfaces, thin films (or foils) and bulk condensed matter.

Due to the worldwide availability of single stage and tandem Van-de-Graff accelerators, electron ejection was widely studied in the corresponding relatively low projectile energy range of keV/u to 1 MeV/u. Studies at 1–400 MeV/u energies are more scarce because they need large accelerator facilities. However, ultra-relativistic projectiles with energies as high as 6.4 TeV were used by Vane et al. (1993), who studied high energy "knock-on" electrons ($E = 0.6$–12 MeV) from collisions of S ions (200 GeV/u) with target electrons in polypropylene targets. New accelerator facilities such as GSI-FAIR will help to close the gap between such ultra-relativistic projectile and "conventional" energies up to 400 MeV/u as studied up to now.

Acknowledgements

We are indebted to many colleagues who contributed to our involvement in ion beam interaction with matter in general and electron emission in particular. It was interesting to discuss and work with you! With our apologies not to name all of you, we thank as representatives Alexander Clouvas (Thessaloniki) and Gaetano Lanzanò (Catania) and their groups, since important parts of the experimental work presented here was obtained in close collaboration with them. Special thanks are due to our former Ph.D. students Matthias Jung, Michaël Beuve and Michel Caron.

References

Baragiola R.A. (Ed.) (1993): Ionization of Solids by Heavy Particles. NATO ASI Series B, Vol. 306. Plenum Publishing Corporation

Barrué F., Chevallier M., Dauvergne D., Kirsch R., Poizat J.C., Ray C., Adoui L., Cassimi A., Rothard H., Toulemonde M., Cohen C., L'Hoir A., Vernhet D., Demonchy C., Giot L., Mittig W., Pita S., Roussel-Chomaz P. and Billebaud A. (2004): Electron emission induced by fast heavy ions in a thin Silicon crystal. Phys Rev A **70**, 032902

Bechthold U., Ullrich J., Ramm U., Kraft G., Hagmann S., Schultz D.R., Reinhold C.O. and Schmidt-Böcking H. (1998): Binary-encounter electron emission after fast heavy-ion impact on complex rare- and molecular-gas targets. Phys Rev A **58**, 1971–1979

Benka O. and Steinbatz M. (2003): Temperature dependence of the electron and ion induced electron emission yield of Al, Cu and Ag. Nucl Instrum Meth B **201**, 296–404

Benka O., Schinner A., Fink T. and Pfaffenlehner M. (1995): Electron emission yield of Al, Cu, and Au for the impact of swift bare ions. Phys Rev A **52**, 3959–3965

Beuve M., Caron M., Gervais B. and Rothard H. (2000): Charge dependence of electron emission in swift heavy ion collisions with carbon. Phys Rev B **62**, 8818–8823

Beuve M., Caron M., Gervais B., Rothard H., Clouvas A. and Potiriadis C. (2001): Experimental study and Monte Carlo simulation of the correlation between electron emission and stopping power for swift proton impact on amorphous carbon target. Eur Phys J D **15**, 293–300

Beuve M., Caron M., Fainstein P.D., Galassi M., Gervais B., Rivarola R.D. and Rothard H. (2002): Monte Carlo simulation of electron emission induced by swift highly charged ions: Beyond the linear response approximation. Eur Phys J D **21**, 125–135

Borovsky J.E. and Suszcynsky D.M. (1991): Reduction of secondary-electron yields by collective electric fields within metals. Phys Rev A **43**, 1433–1440

Breinig M., Elston S.B., Huldt S., Liljeby L., Vane C.R., Berry S.D., Glass G.A., Schauer M., Sellin I.A., Alton G.D., Datz S., Overbury S., Laubert R. and Suter M. (1982): Experiments concerning electron capture and loss to the continuum and convoy electron production by highly ionized projectiles in the 0.7–8.5 MeV/u range traversing the rare gases, polycrystalline solids, and axial channels in gold. Phys Rev A **25**, 3015–3048

Brice D.K. and Sigmund P. (1980): Secondary electron spectra from dielectric theory. K Dan Vidensk Selsk Mat Fys Medd **40, no. 8**

Brusilovsky B.A. (1985): Directional effects in kinetic ion-electron emission. Vacuum **36**, 595–615

Burgdörfer J. and Gibbons J. (1990): Electron transport in the presence of a Coulomb field. Phys Rev A **42**, 1206–1221

Burgdörfer J., Wang J. and Müller J. (1989): Forward electron production in antimatter-solid collisions. Phys Rev Lett **62**, 1599–1602

Burkhard M., Rothard H., Biedermann C., Kemmler J., Koschar P. and Groeneveld K.O. (1987a): Strong convoy electron yield dependence on surface properties. Nucl Instrum Meth B **24/25**, 143–146

Burkhard M., Rothard H., Biedermann C., Kemmler J., Kroneberger K., Koschar P., Heil O. and Groeneveld K.O. (1987b): Heavy-ion-induced shock electrons from sputter-cleaned solid surfaces. Phys Rev Lett **58**, 1773–1775

Caron M., Rothard H., Beuve M. and Gervais B. (2001): Shape analysis of Auger electron spectra induced by highly charged ion impact on carbon. Phys Scripta T **92**, 281–283

Caron M., Rothard H., Toulemonde M., Beuve M. and Gervais B. (2006): Theoretical and experimental study of electronic temperatures in heavy ion tracks from Auger electron spectra and thermal spike calculations. Nucl Instrum Meth B **245**, 36–46

Cazaux J. (2006): E-induced secondary electron emission yield of insulators and the charging effect. Nucl Instrum Meth B **244**, 307–322

Chung M.S. and Everhart T.E. (1977): Role of plasmon decay in secondary electron emission in the nearly-free-electron metals. Application to aluminium. Phys Rev B **15**, 4699–4715

Clouvas A., Potiriadis C., Rothard H., Hofmann D., Wünsch R., Groeneveld K.O., Katsanos A. and Xenoulis A.C. (1997): Role of projectile electrons in secondary electron emission from solid surfaces under fast ion bombardment. Phys Rev B **55**, 12086–12098

Cohen C. and Dauvergne D. (2004): High energy ion channeling: Principles and typical applications. Nucl Instrum Meth B **225**, 40–71

De Filippo E., Lanzanò G., Rothard H., Volant C., Aiello S., Anzalone A., Arena N., Geraci M., Giustolisi F. and Pagano A. (2004): Fast electron ejection from C, Ni, Ag and Au foils by $^{36}Ar^{18+}$ (95 MeV/u): Measurement of absolute cross sections. Eur Phys J A **21**, 169–174

Devooght J., Dubus A. and Dehaes J.C. (1987): Improved age-diffusion model for low-energy electron transport in solids. I. Theory. Phys Rev B **36**, 5093–5109

Devooght J., Dehaes J.C., Dubus A., Cailler M., Ganachaud J.P., Rösler M. and Brauer W. (1991): Particle Induced Electron Emission I. Springer Tracts in Modern Physics, Vol. 122

Drexler C.G. and DuBois R.D. (1996): Energy- and angle-differential yields of electron emission from thin carbon foils after fast proton impact. Phys Rev A **53**, 1630–1636

DuBois R.D. and Drexler C.G. (1994): Electron emission from fast ion impact on thin metal foils: Implications of these data for development of track structure models. In: Varma M.N. and Chatterjee A. (Eds.), Computational Approaches in Molecular Radiation Biology. Plenum Press, New York, pp 49–63

Dubus A., Dehaes J.C., Ganachaud J.P., Hafni A. and Cailler M. (1993): Monte Carlo evaluation of the influence of the interaction cross sections on the secondary-electron-emission yields from polycrystalline aluminum targets. Phys Rev B **47**, 11056–11073

Echenique P.M., Ritchie R.H. and Brandt W. (1979): Spatial excitation patterns induced by swift ions in condensed matter. Phys Rev B **20**, 2567–2580

Fallavier M. (1996): Secondary electron emission of solids by impact of molecular ions and clusters. Nucl Instrum Meth B **112**, 72–78

Füchtbauer C. (1906a): Über eine von Kanalstrahlen erzeugte Sekundär-Strahlung und über eine Reflexion der Kanalstrahlen. Phys Zeitschr **7, no. 5**, 153–157

Füchtbauer C. (1906b). Über die Geschwindigkeit der von Kanalstrahlen und von Kathodenstrahlen beim Auftreffen auf Metalle erzeugten negativen Strahlen. Phys Zeitschr **7, no. 21**, 748–750

Gervais B., Beuve M., Caron M. and Rothard H. (2003): Saturation effects in highly charged ion interaction with thin carbon foils. Nucl Instrum Meth B **205**, 835–840

Griepenkerl K., Schäfer A. and Greiner W. (1995): Mach schock waves and surface effects in metals. J Phys: Condens Matter **7**, 9465–9473

Hasselkamp D., Hippler S., Scharmann A. and Schmehl T. (1990): Electron emission from clean solid surfaces by fast ions, Ann Phys **47** (7. Folge), 555–567

Hasselkamp D., Rothard H., Groeneveld K.O., Kemmler J., Varga P. and Winter Hp. (1991): Particle Induced Electron Emission II, Springer Tracts in Modern Physics, Vol. 123

Jakubassa-Amundsen D.H.(1997): Relativistic theory for binary encounter electron emission. J Phys B: At Mol Opt Phys **30**, 365–385

Juaristi J.I., Rösler M. and García de Abajo F.J. (1998): Contribution of the excitation of conduction band electrons to the kinetic electron emission induced by slow ions in metals. Phys Rev B **58**, 15838–15846

Jung M., Rothard H., Gervais B., Grandin J.P., Clouvas A. and Wünsch R. (1996): Transport of electrons induced by highly charged Ni (74 MeV/u) and Cu (9.6 MeV/u) ions in carbon: A study of target thickness dependent electron yields. Phys Rev A **54**, 4153–4161

Koyama A., Benka O., Sasa Y. and Uda M.(1986): Energy spectra of secondary electrons from Al induced by heavy-ion impact. Phys Rev B **34**, 8150–8152

Kozochina A.A., Leonas V.B. and Fine V.E. (1993): Statistics of heavy particle-induced electron emission from a foil. In: Baragiola R.A. (Ed.), Ionization of Solids by Heavy Particles. NATO ASI Series B, Vol. 306. Plenum Publishing Corporation, pp 223–237

Kraft G. (2000): Tumor therapy with heavy charged particles. Progr Part Nucl Phys **45**, S473–S544

Kudo H. (2001): Ion-Induced Electron Emission from Crystalline Solids. Springer Tracts in Modern Physics, Vol. 175

Lanzanò G., De Filippo E., Aiello S., Geraci M., Pagano A., Cavallaro Sl., LoPiano F., Pollaco E.C., Volant C., Vuillier S., Beck C., Mahboub D., Nouicer R., Politi G., Rothard H. and Jakubassa-Amundsen D.H. (1998): Fast electron production in atomic collisions induced by 77 A-MeV ^{40}Ar ions studied with a multidetector. Phys Rev A **58**, 3634–3641

Lanzanò G., De Filippo E., Mahboub D., Rothard H., Aiello S., Anzalone A., Cavallaro Sl., Elanique A., Geraci E., Geraci M., Giustolisi F., Pagano A. and Politi G. (1999): Fast electron production at intermediate energies: Evidence for Fermi shuttle acceleration and for deviations from simple relativistic kinematics. Phys Rev Lett **83**, 4518–4521

Lanzanò G., De Filippo E., Anzalone A., Arena N., Geraci M., Giustolisi F., Pagano A., Rothard H. and Volant C. (2003): Recent results on fast intermediate velocity electron production induced by 19+ 45 A.MeV ^{58}Ni highly charged ions on thin solid targets. Nucl Instrum Meth B **205**, 841–846

Lencinas S., Burgdörfer J., Kemmler J., Heil O., Kroneberger K., Keller N., Rothard H. and Groeneveld K.O. (1990): Transport of fast electrons through thin foils. Phys Rev A **41**, 1435–1443

Neelavathi V.N., Ritchie R.H. and Brandt W. (1974): Bound electron states in the wake of swift ions in solids. Phys Rev Lett **33**, 302–305

Neugebauer R., Wünsch R., Jalowy T., Groeneveld K.O., Rothard H., Clouvas A. and Potiriadis C. (1999): Secondary electron emission near the electronic stopping power maximum. Phys Rev B **59**, 11113–11116

Rösler M. and Brauer W. (1981): Theory of secondary electron emission. I. General theory for nearly-free-electron metals. Phys Stat Sol (b) **104**, 161

Rösler M. and Brauer W. (1988): Theory of electron emission from solids by proton and electron bombardment. Phys Stat Sol (b) **148**, 213

Rothard H. (2004): Electron ejection by heavy particles as precursor of track formation in condensed matter. Nucl Instrum Meth B **225**, 27–39

Rothard H., Schosnig M., Kroneberger K. and Groeneveld K.O. (1992): Ion induced electron emission study of high Tc superconductors and phase transitions. Phys Rev B **46**, 11847–11853

Rothard H., Jakubassa-Amundsen D.H. and Billebaud A. (1998a): Solid state effects in binary encounter electron emission from 13.6 MeV/u Ar^{17+} collisions with C, Al, Cu and Au foils. J Phys B: At Mol Opt Phys **31**, 1563–1578

Rothard H., Jung M., Caron M., Grandin J.P., Gervais B., Billebaud A., Clouvas A. and Wünsch R. (1998b): Strong projectile dependent forward/backward asymmetry of electron ejection by swift heavy ions in solids. Phys Rev A **57**, 3660–3664

Rothard H., Lanzanò G., Jakubassa-Amundsen D.H., De Filippo E. and Mahboub D. (2001): Theory and measurement of absolute doubly differential cross sections of binary encounter electron ejection in collisions of swift heavy ions with solids. J Phys B: At Mol Opt Phys **43**, 3261–3274

Rothard H., Lanzanò G., De Filippo E. and Volant C. (2005): Fermi shuttle acceleration in atomic collisions: The case of ion induced electron emission. Nucl Instrum Meth B **230**, 419–425

Rothard H., Moshammer R., Ullrich J., Kollmus H., Mann R., Hagmann S. and Zouros T.J.M. (2007): Differential multi-electron emission induced by swift highly charged gold ions penetrating carbon foils. Nucl Instrum Meth B, to appear

Schäfer W., Stöcker H., Müller B. and Greiner W. (1980): Mach shock electron distributions from solids. Z Phys B **36**, 319–322

Schiwietz G., Biersack J.P., Schneider D., Stolterfoht N., Fink D., Montemayor V. and Skogvall B. (1990): Investigation of δ-electron emission in collisions of highly charged fast Ne projectiles with carbon-foil targets. Phys Rev B **41**, 6262–6271

Schiwietz G., Grande P., Skogvall B., Biersack J.P., Köhrbrück R., Sommer K., Schmoldt A., Goppelt P., Kadar I., Ricz S. and Stettner U. (1992): Influence of nuclear track potentials in insulators on the emission of target Auger electrons. Phys Rev Lett **69**, 628–631

Schiwietz G., Xiao G., Grande P.L., Luderer E., Pazirandeh R. and Stettner U. (1999): Determination of the electron temperature in the thermal spike of amorphous carbon. Europhys Lett **47**, 384–390

Schiwietz G., Xiao G., Luderer E. and Grande P.L. (2000): Auger electrons from ion tracks. Nucl Instrum Meth B **164/165**, 353–364

Schiwietz G., Czerski K., Roth M., Staufenbiel F. and Grande P.L. (2004): Femtosecond dynamics – snapshots of the early ion-track evolution. Nucl Instrum Meth B **226**, 683–704

Schou J. (1980): Transport theory for kinetic emission of secondary electrons from solids. Phys Rev B **22**, 2141–2174

Sigmund P. and Tougaard S. (1981). Electron emission from solids during ion bombardment: Theoretical aspects. In: Taglauer E. and Heiland W. (Eds), Inelastic Particle-Surface Collisions. Springer Series in Chemical Physics, Vol. 17, pp 2–37

Smidts O.F., Dubus A., Vidović Z., Billebaud A., Fallavier M., Kirsch R., Poizat J.C., Remillieux J. and Rösler M. (1999): Theoretical and experimental study of the correlation between forward and backward electron emissions induced by H^0 or H^+ projectiles incident on carbon foils. Nucl Instrum Meth B **157**, 239–245

Sternglass E.J. (1957): Theory of secondary electron emission by high-speed ions. Phys Rev **108**, 1–12

Spohr R. (1990): Ion Tracks and Microtechnology. Friedr. Vieweg & Sohn Verlags GmbH, Braunschweig

Staufenbiel F., Schiwietz G., Czerski K., Roth M. and Grande P.L. (2005): Electronic energy-density effects in ion tracks of metals. Nucl Instrum Meth B **230**, 426–430

Stolterfoht N., (1987): High resolution Auger spectroscopy in energetic ion collisions. Phys Rep **146**, 315–424

Stolterfoht N., Dubois R.D. and Rivarola R.D., (1997): Electron Emission in Heavy-Ion-Atom Collision. Springer Series on Atoms and Plasmas, Vol. 20

Sulik B., Koncz Cs., Tökési K., Orbán A. and Berényi D. (2002): Evidence for Fermi-shuttle ionization in intermediate velocity C^++Xe collisions. Phys Rev Lett **88**, 073201

Sulik B., Stolterfoht N., Hellhammer R., Pésiç Z., Koncz Cs., Tökési K. and Berényi D. (2003): Fermi-shuttle acceleration of electrons in ion–matter interaction. Nucl Instrum Meth B **212**, 33–44

Tougaard S. and Sigmund P. (1982): Influence of elastic and inelastic scattering on energy spectra of electrons emitted from solids. Phys Rev B **25**, 4452–4460

Ullrich J., Moshammer R., Dorn A., Dörner R., Schmidt L.P. and Schmidt-Böcking H. (2003): Recoil-ion and electron momentum spectroscopy: Reaction-microscopes. Rep Prog Phys **66**, 1463–1545

Vane C.R., Datz S., Dittner P.F., Krause H.F., Schuch R., Gao H. and Hutton R. (1993): Knock-on electrons produced in collisions of 6.4 TeV sulfur ions with fixed targets. Nucl Instrum Meth B **79**, 26–29

Vidović Z., Billebaud A., Fallavier M., Kirsch R., Poizat J.C. and Remillieux J. (1997): Backward- and forward-electron-emission measurements for MeV H^0 projectiles incident on thin carbon foils: Correlation with the charge state of the emergent projectile. Phys Rev A **56**, 4807–4814

Yamazaki Y., Kuroki K., Komaki K.J., Andersen L.H., Horsdal-Pedersen E., Hvelplund P., Knudsen H., Moller S.P., Uggerhoj E. and Elsener K. (1990): Measurements of electron spectra in the forward direction in slow antiproton-carbon foil collisions. J Phys Soc of Japan **59**, 2643–2646

Yamazaki Y., Kuroki K., Azuma T., Komaki K., Watanabe H., Kakutani N., Hasegawa T., Sekiguchi M. and Hattori T. (1993): Correlated electron emission from thin carbon foils bombarded by 1.8 MeV/u Ar ions. Phys Rev Lett **70**, 2702–2705

Weng M.S., Schinner A., Sharma A. and Sigmund P. (2006): Primary electron spectra from swift heavy-ion impact: Scaling relations and estimates from modified Bohr theory. Eur Phys J D **39**, 209–221

Willis R.F., Fitton B. and Painter G.S. (1974): Secondary-electron emission spectroscopy and the observation of high-energy excited states in graphite: Theory and experiment. Phys Rev B **9**, 1926–1937

Xiao G., Schiwietz G., Grande P.L., Stolterfoht N., Schmoldt A., Grether M., Kohrbruck R., Spieler A. and Stettner A. (1997): Indications of nuclear-track-guided electrons induced by fast heavy ions in insulators. Phys Rev Lett **79**, 1821–1824

Zäpfel T., Hagmann S., Rothard H., Ullrich J., Kraft G., Schmidt-Böcking H. and Groeneveld K.O. (2002): Experimental study of electron ejection by heavy ion irradiation of solids: Observation of forward and backward emitted electron jets. Nucl Instrum Meth B **193**, 651–655